# Associating long-term $\gamma$ -ray variability with the superorbital period of LS I $+61^{\circ}303$

- M. Ackermann<sup>1</sup>, M. Ajello<sup>2</sup>, J. Ballet<sup>3</sup>, G. Barbiellini<sup>4,5</sup>, D. Bastieri<sup>6,7</sup>, R. Bellazzini<sup>8</sup>, E. Bonamente<sup>9,10</sup>, T. J. Brandt<sup>11</sup>, J. Bregeon<sup>8</sup>, M. Brigida<sup>12,13</sup>, P. Bruel<sup>14</sup>, R. Buehler<sup>1</sup>, S. Buson<sup>6,7</sup>, G. A. Caliandro<sup>15†</sup>, R. A. Cameron<sup>16</sup>, P. A. Caraveo<sup>17</sup>, J. M. Casandjian<sup>3</sup>. E. Cavazzuti<sup>18</sup>, C. Cecchi<sup>9,10</sup>, A. Chekhtman<sup>19</sup>, J. Chiang<sup>16</sup>, G. Chiaro<sup>7</sup>, S. Ciprini<sup>18,20</sup>, R. Claus<sup>16</sup>, J. Cohen-Tanugi<sup>21</sup>, L. R. Cominsky<sup>22</sup>, J. Conrad<sup>23,24,25,26</sup>, S. Cutini<sup>18,20</sup>, M. Dalton<sup>27</sup>, F. D'Ammando<sup>28</sup>, A. de Angelis<sup>29</sup>, P. R. den Hartog<sup>16</sup>, F. de Palma<sup>12,13</sup>. C. D. Dermer<sup>30</sup>, S. W. Digel<sup>16</sup>, L. Di Venere<sup>16</sup>, P. S. Drell<sup>16</sup>, R. Dubois<sup>16</sup>, C. Favuzzi<sup>12,13</sup> S. J. Fegan<sup>14</sup>, E. C. Ferrara<sup>11</sup>, W. B. Focke<sup>16</sup>, A. Franckowiak<sup>16</sup>, S. Funk<sup>16</sup>, P. Fusco<sup>12,13</sup>, F. Gargano<sup>13</sup>, D. Gasparrini<sup>18,20</sup>, S. Germani<sup>9,10</sup>, N. Giglietto<sup>12,13</sup>, F. Giordano<sup>12,13</sup>, M. Giroletti<sup>28</sup>, T. Glanzman<sup>16</sup>, G. Godfrey<sup>16</sup>, I. A. Grenier<sup>3</sup>, S. Guiriec<sup>11,31</sup>, D. Hadasch<sup>15†</sup>, Y. Hanabata<sup>32</sup>, A. K. Harding<sup>11</sup>, M. Hayashida<sup>16,33</sup>, E. Hays<sup>11</sup>, A. B. Hill<sup>16,34,35</sup>, D. Horan<sup>14</sup>, R. E. Hughes<sup>36</sup>, T. Jogler<sup>16</sup>, G. Jóhannesson<sup>38</sup>, A. S. Johnson<sup>16</sup>, T. J. Johnson<sup>39</sup>, T. Kawano<sup>32</sup>, M. Kerr<sup>16</sup>, J. Knödlseder<sup>40,41</sup>, M. Kuss<sup>8</sup>, J. Lande<sup>16</sup>. S. Larsson<sup>23,24,42</sup>, L. Latronico<sup>43</sup>, M. Lemoine-Goumard<sup>27,44</sup>, J. Li<sup>15,44</sup>, F. Longo<sup>4,5</sup>, M. N. Lovellette<sup>30</sup>, P. Lubrano<sup>9,10</sup>, M. Mayer<sup>1</sup>, M. N. Mazziotta<sup>13</sup>, J. E. McEnery<sup>11,45</sup> P. F. Michelson<sup>16</sup>, T. Mizuno<sup>46</sup>, M. E. Monzani<sup>16</sup>, A. Morselli<sup>47</sup>, I. V. Moskalenko<sup>16</sup>, S. Murgia<sup>16</sup>, R. Nemmen<sup>11</sup>, E. Nuss<sup>21</sup>, T. Ohsugi<sup>46</sup>, A. Okumura<sup>16,48</sup>, M. Orienti<sup>28</sup>, E. Orlando<sup>16</sup>, J. F. Ormes<sup>49</sup>, D. Paneque<sup>50,16</sup>, A. Papitto<sup>15</sup>, J. S. Perkins<sup>11,51,52</sup>, M. Pesce-Rollins<sup>8</sup>, F. Piron<sup>21</sup>, G. Pivato<sup>7</sup>, S. Rainò<sup>12,13</sup>, R. Rando<sup>6,7</sup>, M. Razzano<sup>8,53</sup>, N. Rea<sup>15</sup>, A. Reimer<sup>54,16</sup>, O. Reimer<sup>54,16</sup>, J. D. Scargle<sup>55</sup>, A. Schulz<sup>1</sup>, C. Sgrò<sup>8</sup>, E. J. Siskind<sup>56</sup>, G. Spandre<sup>8</sup>, P. Spinelli<sup>12,13</sup>, H. Takahashi<sup>32</sup>, J. G. Thayer<sup>16</sup>, J. B. Thayer<sup>16</sup>, M. Tinivella<sup>8</sup>, D. F. Torres<sup>15,57,†</sup>, G. Tosti<sup>9,10</sup>, E. Troja<sup>11,31</sup>, Y. Uchiyama<sup>58</sup>, T. L. Usher<sup>16</sup>, J. Vandenbroucke<sup>16</sup>, V. Vasileiou<sup>21</sup>, G. Vianello<sup>16,59</sup>, V. Vitale<sup>47,60</sup>, M. Werner<sup>54</sup>, B. L. Winer<sup>36</sup>, K. S. Wood<sup>30</sup>
  - † A. Caliandro (andrea.caliandro@ieec.uab.es), D. Hadasch (hadasch@ieec.uab.es), D. F. Torres (dtorres@ieec.uab.es)

<sup>&</sup>lt;sup>1</sup>Deutsches Elektronen Synchrotron DESY, D-15738 Zeuthen, Germany

<sup>&</sup>lt;sup>2</sup>Space Sciences Laboratory, 7 Gauss Way, University of California, Berkeley, CA 94720-7450, USA

<sup>&</sup>lt;sup>3</sup>Laboratoire AIM, CEA-IRFU/CNRS/Université Paris Diderot, Service d'Astrophysique, CEA Saclay, 91191 Gif sur Yvette, France

<sup>&</sup>lt;sup>4</sup>Istituto Nazionale di Fisica Nucleare, Sezione di Trieste, I-34127 Trieste, Italy

<sup>&</sup>lt;sup>5</sup>Dipartimento di Fisica, Università di Trieste, I-34127 Trieste, Italy

<sup>&</sup>lt;sup>6</sup>Istituto Nazionale di Fisica Nucleare, Sezione di Padova, I-35131 Padova, Italy

<sup>&</sup>lt;sup>7</sup>Dipartimento di Fisica e Astronomia "G. Galilei", Università di Padova, I-35131 Padova, Italy

<sup>&</sup>lt;sup>8</sup>Istituto Nazionale di Fisica Nucleare, Sezione di Pisa, I-56127 Pisa, Italy

<sup>&</sup>lt;sup>9</sup>Istituto Nazionale di Fisica Nucleare, Sezione di Perugia, I-06123 Perugia, Italy

<sup>&</sup>lt;sup>10</sup>Dipartimento di Fisica, Università degli Studi di Perugia, I-06123 Perugia, Italy

<sup>&</sup>lt;sup>11</sup>NASA Goddard Space Flight Center, Greenbelt, MD 20771, USA

<sup>&</sup>lt;sup>12</sup>Dipartimento di Fisica "M. Merlin" dell'Università e del Politecnico di Bari, I-70126 Bari, Italy

<sup>&</sup>lt;sup>13</sup>Istituto Nazionale di Fisica Nucleare, Sezione di Bari, 70126 Bari, Italy

<sup>&</sup>lt;sup>14</sup>Laboratoire Leprince-Ringuet, École polytechnique, CNRS/IN2P3, Palaiseau, France

<sup>&</sup>lt;sup>15</sup>Institute of Space Sciences (IEEE-CSIC), Campus UAB, 08193 Barcelona, Spain

<sup>&</sup>lt;sup>16</sup>W. W. Hansen Experimental Physics Laboratory, Kavli Institute for Particle Astrophysics and Cosmology, Department of Physics and SLAC National Accelerator Laboratory, Stanford University, Stanford, CA 94305, USA

 $<sup>^{17} \</sup>mathrm{INAF}\text{-}\mathrm{Istituto}$ di Astrofisica Spaziale e Fisica Cosmica, I-20133 Milano, Italy

<sup>&</sup>lt;sup>18</sup>Agenzia Spaziale Italiana (ASI) Science Data Center, I-00044 Frascati (Roma), Italy

<sup>&</sup>lt;sup>19</sup>Center for Earth Observing and Space Research, College of Science, George Mason University, Fairfax, VA 22030, resident at Naval Research Laboratory, Washington, DC 20375, USA

<sup>&</sup>lt;sup>20</sup>Istituto Nazionale di Astrofisica - Osservatorio Astronomico di Roma, I-00040 Monte Porzio Catone (Roma), Italy

<sup>&</sup>lt;sup>21</sup>Laboratoire Univers et Particules de Montpellier, Université Montpellier 2, CNRS/IN2P3, Montpellier, France

<sup>&</sup>lt;sup>22</sup>Department of Physics and Astronomy, Sonoma State University, Rohnert Park, CA 94928-3609, USA

<sup>&</sup>lt;sup>23</sup>Department of Physics, Stockholm University, AlbaNova, SE-106 91 Stockholm, Sweden

<sup>&</sup>lt;sup>24</sup>The Oskar Klein Centre for Cosmoparticle Physics, AlbaNova, SE-106 91 Stockholm, Sweden

 $<sup>^{25}</sup>$ Royal Swedish Academy of Sciences Research Fellow, funded by a grant from the K. A. Wallenberg Foundation

<sup>&</sup>lt;sup>26</sup>The Royal Swedish Academy of Sciences, Box 50005, SE-104 05 Stockholm, Sweden

<sup>&</sup>lt;sup>27</sup>Centre d'Études Nucléaires de Bordeaux Gradignan, IN2P3/CNRS, Université Bordeaux 1, BP120, F-33175 Gradignan Cedex, France

<sup>&</sup>lt;sup>28</sup>INAF Istituto di Radioastronomia, 40129 Bologna, Italy

<sup>&</sup>lt;sup>29</sup>Dipartimento di Fisica, Università di Udine and Istituto Nazionale di Fisica Nucleare, Sezione di Trieste, Gruppo Collegato di Udine, I-33100 Udine, Italy

<sup>&</sup>lt;sup>30</sup>Space Science Division, Naval Research Laboratory, Washington, DC 20375-5352, USA

<sup>&</sup>lt;sup>31</sup>NASA Postdoctoral Program Fellow, USA

<sup>&</sup>lt;sup>32</sup>Department of Physical Sciences, Hiroshima University, Higashi-Hiroshima, Hiroshima 739-8526, Japan

<sup>&</sup>lt;sup>33</sup>Department of Astronomy, Graduate School of Science, Kyoto University, Sakyo-ku, Kyoto 606-8502, Japan

<sup>&</sup>lt;sup>34</sup>School of Physics and Astronomy, University of Southampton, Highfield, Southampton, SO17 1BJ, UK

<sup>&</sup>lt;sup>35</sup>Funded by a Marie Curie IOF, FP7/2007-2013 - Grant agreement no. 275861

 $<sup>^{36} \</sup>mbox{Department}$  of Physics, Center for Cosmology and Astro-Particle Physics, The Ohio State University, Columbus, OH 43210, USA

<sup>&</sup>lt;sup>37</sup>Science Institute, University of Iceland, IS-107 Reykjavik, Iceland

 $<sup>^{38}</sup>$ National Research Council Research Associate, National Academy of Sciences, Washington, DC 20001, resident at Naval Research Laboratory, Washington, DC 20375, USA

<sup>&</sup>lt;sup>39</sup>CNRS, IRAP, F-31028 Toulouse cedex 4, France

<sup>&</sup>lt;sup>40</sup>GAHEC, Université de Toulouse, UPS-OMP, IRAP, Toulouse, France

<sup>&</sup>lt;sup>41</sup>Department of Astronomy, Stockholm University, SE-106 91 Stockholm, Sweden

<sup>&</sup>lt;sup>42</sup>Istituto Nazionale di Fisica Nucleare, Sezione di Torino, I-10125 Torino, Italy

<sup>&</sup>lt;sup>43</sup>Funded by contract ERC-StG-259391 from the European Community

<sup>&</sup>lt;sup>44</sup>Key Laboratory for Particle Astrophysics, Institute of High Energy Physics, Beijing 100049, China

 $<sup>^{45}\</sup>mathrm{Department}$  of Physics and Department of Astronomy, University of Maryland, College Park, MD 20742, USA

 $<sup>^{46}\</sup>mbox{Hiroshima}$  Astrophysical Science Center, Hiroshima University, Higashi-Hiroshima, Hiroshima 739-8526, Japan

<sup>&</sup>lt;sup>47</sup>Istituto Nazionale di Fisica Nucleare, Sezione di Roma "Tor Vergata", I-00133 Roma, Italy

<sup>&</sup>lt;sup>48</sup>Solar-Terrestrial Environment Laboratory, Nagoya University, Nagoya 464-8601, Japan

<sup>&</sup>lt;sup>49</sup>Department of Physics and Astronomy, University of Denyer, Denyer, CO 80208, USA

<sup>&</sup>lt;sup>50</sup>Max-Planck-Institut für Physik, D-80805 München, Germany

## ABSTRACT

Gamma-ray binaries are stellar systems for which the spectral energy distribution (discounting the thermal stellar emission) peaks at high energies. Detected from radio to TeV gamma rays, the  $\gamma$ -ray binary LS I +61°303 is highly variable across all frequencies. One aspect of this system's variability is the modulation of its emission with the timescale set by the  $\sim 26.4960$ -day orbital period. Here we show that, during the time of our observations, the  $\gamma$ -ray emission of LS I +61°303 also presents a sinusoidal variability consistent with the previously-known superorbital period of 1667 days. This modulation is more prominently seen at orbital phases around apastron, whereas it does not introduce a visible change close to periastron. It is also found in the appearance and disappearance of variability at the orbital period in the power spectrum of the data. This behavior could be explained by a quasi-cyclical evolution of the equatorial outflow of the Be companion star, whose features influence the conditions for generating gamma rays. These findings open the possibility to use  $\gamma$ -ray observations to study the outflows of massive stars in eccentric binary systems.

Subject headings: gamma-rays: observations, X-ray binaries (individual: LS I +61°303)

 $<sup>^{51} \</sup>rm Department$  of Physics and Center for Space Sciences and Technology, University of Maryland Baltimore County, Baltimore, MD 21250, USA

<sup>&</sup>lt;sup>52</sup>Center for Research and Exploration in Space Science and Technology (CRESST) and NASA Goddard Space Flight Center, Greenbelt, MD 20771, USA

<sup>&</sup>lt;sup>53</sup>Santa Cruz Institute for Particle Physics, Department of Physics and Department of Astronomy and Astrophysics, University of California at Santa Cruz, Santa Cruz, CA 95064, USA

 $<sup>^{54}</sup>$ Institut für Astro- und Teilchenphysik and Institut für Theoretische Physik, Leopold-Franzens-Universität Innsbruck, A-6020 Innsbruck, Austria

<sup>&</sup>lt;sup>55</sup>Space Sciences Division, NASA Ames Research Center, Moffett Field, CA 94035-1000, USA

<sup>&</sup>lt;sup>56</sup>NYCB Real-Time Computing Inc., Lattingtown, NY 11560-1025, USA

<sup>&</sup>lt;sup>57</sup>Institució Catalana de Recerca i Estudis Avançats (ICREA), Barcelona, Spain

 $<sup>^{58}3\</sup>text{-}34\text{-}1$ Nishi-Ikebukuro,<br/>Toshima-ku, , Tokyo Japan 171-8501

<sup>&</sup>lt;sup>59</sup>Consorzio Interuniversitario per la Fisica Spaziale (CIFS), I-10133 Torino, Italy

<sup>&</sup>lt;sup>60</sup>Dipartimento di Fisica, Università di Roma "Tor Vergata", I-00133 Roma, Italy

## 1. Introduction

LS I +61°303 is one of the few X-ray binaries that have been detected from radio to TeV gamma rays (see Albert et al. 2006 and references therein). It is perhaps the most intriguing one due to the high variability and richness of its phenomenology at all frequencies. LS I +61°303 consists of a Be star of approximately 10 solar masses, and a compact object. Be stars are rapidly rotating B-type stars showing hydrogen Balmer lines in emission in the stellar spectrum, and which lose mass to an equatorial circumstellar disc. The nature of the compact object in LS I +61°303 has been much debated over the past few years: Pulsar wind interaction (see e.g., Maraschi & Treves 1981; Dubus 2006; Zamanov et al. 2001; Torres et al. 2012) and microquasar jets (see Bosch-Ramon & Khangulyan 2009 for a review) have been proposed as the origin of the non-thermal emission. The recent detection of two short (< 0.1 s), highly-luminous (>  $10^{37}$  erg s<sup>-1</sup>), thermal flares (Papitto et al. 2012) have given support to the hypothesis that the compact object in LS I +61°303 is a neutron star, for only highly-magnetized neutron stars have been found to behave in this way.

The flux of LS I +61°303 is seen to be modulated by the orbital period of 26.4960 days (Gregory 2002) at most wavelengths, including at high energies (Torres et al. 2010; Zhang et al. 2010; Abdo et al. 2009; Albert et al. 2008). Orbital modulation of the GeV flux can be understood as a consequence of changing conditions for generation and absorption of gamma rays, which are mostly determined by the orbital geometry; e.g., the viewing angle to the observer and the position of the compact object with respect to the stellar companion. Unless other physical conditions change, we do not expect long-term variability of the emission level at a fixed orbital configuration. In order to investigate LS I +61°303's variability, we analyzed Fermi-Large Area Telescope (LAT) data from the beginning of scientific operations on 2008 August 4 until 2013 March 24. We report on the results in this Letter.

## 2. Data Analysis

We used the LAT Science Tools package (v9r30), which is available from the *Fermi* Science Support Center, as is the LAT data, together with the P7v6 version of the instrument response functions. Only events passing the Pass 7 "Source" class cuts are used in the analysis. All gamma rays with energies > 100 MeV within a circular region of interest (ROI) of 10° radius centered on LS I +61°303 were extracted. To reduce the contamination from the Earth's upper atmosphere time intervals when the Earth limb was in the field of view were excluded, specifically when the rocking angle of the LAT was greater than 52° or when parts of the ROI were observed at zenith angles > 100°. The  $\gamma$ -ray flux of LS I +61°303 plotted in

the light curves of this work are calculated by performing the binned or the unbinned maximum likelihood method, depending on the statistics, by means of the Science Tool gtlike. The spectral-spatial model constructed to perform the likelihood analysis includes all the sources of the second Fermi-LAT point-source catalog (Nolan et al. 2012) (hereafter 2FGL) within 15° of LS I +61°303. The spectral parameters were fixed to the catalog values, except for the sources within 3° of LS I +61°303. For these latter sources, the flux normalization was left free. LS I +61°303 was modeled with an exponentially cut off power-law spectral shape. All its spectral parameters were allowed to vary (see Hadasch et al. 2012 for further details). The models adopted for the Galactic diffuse emission (gal\_2yearp7v6\_v0.fits) and isotropic backgrounds (iso\_p7v6source.txt) were those recommended by the LAT team.<sup>1</sup>

Systematic errors mainly originate in the uncertainties in the effective area of the LAT, as well as in the Galactic diffuse emission model. The current estimate of the uncertainties of the effective area is 10% at 100 MeV, decreasing to 5% at 560 MeV and increasing to 10% at 10 GeV and above. We assume linear extrapolations, in log space, between the quoted energies. The systematic effect is estimated by repeating the likelihood analysis using modified instrument response functions that bracket the "P7SOURCE\_V6" effective areas. Specifically, they are a set of Instrument Response Functions in which the effective area has been modified considering its uncertainty as a function of energy in order to maximally affect a specific spectral parameter. In order to conservatively take into account the effect due to the uncertainties of the Galactic diffuse emission model, the likelihood fits are repeated changing the normalization of the Galactic diffuse model artificially by  $\pm 6\%$ . We have found flux systematic errors (for energies above 100 MeV) on the order of 9%, similar to the ones reported in Hadasch et al. 2012.

## 3. Results

Fig. 1 shows the orbitally-folded light curve of LS I +61°303 from 2008 August 4 to 2013 March 24. It shows a trend for the maximum of the  $\gamma$ -ray emission to appear near periastron (phases around 0.3), as in Hadasch et al. 2012, and significant  $\gamma$ -ray flux variability at fixed orbital phases.

We explore the possibility that the observed long term  $\gamma$ -ray variability could be re-

<sup>&</sup>lt;sup>1</sup>A description of these models is available from the *Fermi* Science Support Center: \protecthttp://fermi.gsfc.nasa.gov/ssc/data/access/lat/BackgroundModels.html.

<sup>&</sup>lt;sup>2</sup>The released Pass 7 Instrument Response Functions are documented here: http://www.slac.stanford.edu/exp/glast/groups/canda/lat\_Performance.htm.

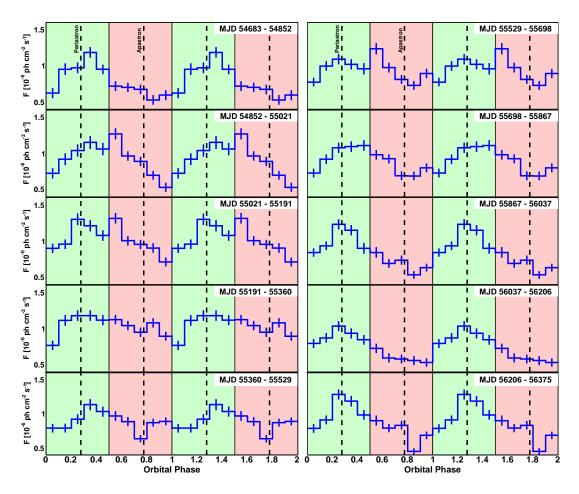


Fig. 1.— Gamma-ray flux from LS I +61°303 folded on the orbital period. The data are repeated over two cycles for clarity. Photons with energies above 100 MeV, as measured by Fermi-LAT are considered. The measurements cover the period from 2008 August 4 to 2013 March 24, from the top left panel to the bottom right. Each panel spans an equal interval of 169.2 days. The position of periastron and apastron are marked with dashed vertical lines (the ephemeris of Aragona et al. 2009 is used). The two background colors correspond to the periastron (orbital phases 0.0–0.5) and apastron (orbital phases 0.5-1.0) regions of the orbit.

lated to the superorbital period of  $1667\pm 8$  days as reported in radio and optical frequencies (Gregory 2002). A variability signature with this period was also found along several years of X-ray observations (Li et al. 2012; Chernyakova et al. 2012). Fig. 2 shows the long-term evolution of the average  $\gamma$ -ray flux; we use the superorbital period of Gregory (2002) to translate time to superorbital phase. The probability that this evolution is a random result out of a uniform distribution is  $< 1.1 \times 10^{-12}$  ( $\chi^2$ , ndf = 75.8, 9).

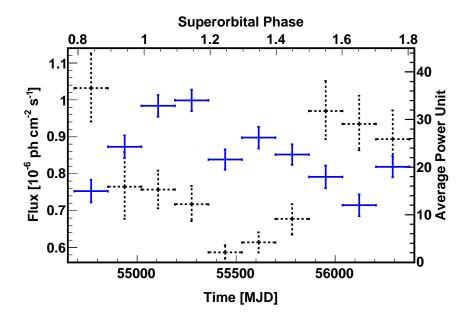


Fig. 2.— Long-term evolution of the average  $\gamma$ -ray flux (above 100 MeV) from LS I +61°303 (blue points, left y-axis scale). The superorbital phase is shown in the top axis. The right y-axis scale and the black dashed points show the long-term evolution of the power at the orbital period found in the Lomb-Scargle periodogram.

To check for a possible long-term modulation of the  $\gamma$ -ray flux at any orbital configuration, we have separated the data in orbital bins, and plotted the fluxes against the superorbital phase, as shown in Fig. 3. The black line in each of the panels of Fig. 3 represents a sinusoidal function fit to the data points. The period of this function has been kept (in all panels) at the value of the superorbital period found in radio (1667 days). Thus, the function we use to fit the data has three parameters: average flux level, amplitude, and phase. We have also fitted a constant line for comparison.

Table 1 shows the quality of the fitting results corresponding to Fig. 3. It has the following columns: the system's orbital phase, the corresponding  $\chi^2$  and dof as well as the probability that the data are described by either a constant or a sinusoidally varying flux, and finally the probability that the improvement found when fitting a sinusoid instead of a constant is produced by chance. To obtain the latter we consider the likelihood ratio test (Mattox et al. 1996). The test is performed by computing the ratio  $2 \times \Delta log(Likelihood)$  for the two hypotheses (constant and sinusoidal) and assuming that for a chance coincidence the ratios are  $\chi^2$ -distributed according to the difference in the degrees of freedom between the two hypotheses. Thus, if the hypothesis of a constant is true, the likelihood ratio  $R = -2 \ln(L(constant)/L(sine))$  is approximately  $\chi^2$ -distributed with 2 degrees of freedom. The

probability that one hypothesis is preferred over the other is defined as  $P = \int_0^{R_{meas}} p(\chi^2) d\chi^2$  where  $p(\chi^2)$  is the  $\chi^2$  probability density function and  $R_{meas}$  the measured value of R. The constant hypothesis will be rejected (and the sinusoidal will be accepted) if P is greater than the confidence level, which is set to 95%. In Table 1, the last column states the probability that the fit improvement (of a sine over a constant) is happening by chance (thus, 1 - P).

Table 1 also shows the sinusoidal fit parameters corresponding to the right-hand panels of Fig. 3. The functional form of the fit is  $F_0 + A \times \sin((t - T_0)/T - \phi) \times 2\pi)$ . Here,  $T_0$  and T are the zero time ( $T_0 = \text{MJD } 43366.275$ ) and the period (always kept fixed at 1667 days in all panels) of the superorbit, respectively (both as in Gregory 2002), t is the time,  $F_0$  is the average flux level, A is the amplitude, and  $\phi$  represents the phase shift in the superorbit. The choice of a sinusoidal function for fitting the data is not based on any a priori physical expectation; the superorbital variability could be periodic but have a different shape. However, any periodic function could be described by a series of sines. Thus, fitting with just one sinusoidal function as done above is motivated by the relatively low number of data points.

No strong variability is found at orbital phases 0.0–0.5, while it is clearly present in the range 0.5–1.0. Concurrently, data at the orbital phases 0.0 to 0.5 are not significantly better-represented by a sine than by a constant. However, this is not the case for the data at the orbital phases 0.5 to 1.0. The probability that the sinusoidal fit improvement occurs by chance is less than  $1.0 \times 10^{-7}$  at orbital phases 0.5–0.6, 0.6–0.7, 0.8–0.9, and 0.9–1.0; and  $1.4 \times 10^{-5}$  at orbital phases 0.7-0.8. Whereas the sinusoidal variation is always a better fit in this part of the orbit, the amplitude of the fit is maximal in orbital phases before and after the apastron.

In order to test for the appearance/disappearance of the orbital signature in gamma rays, we subdivided the data into the same time intervals of Fig. 1 and applied the Lomb-Scargle periodogram technique (Lomb 1976; Scargle 1982) to each of them. To calculate the power spectrum the event selection was restricted to a ROI of 3° radius centered on LS I +61°303. The selected events were used to create a light curve of weighted counts over exposure with equally spaced time bins of 2.4 hours width. The weight associated to each event corresponds to the probability that the  $\gamma$ -ray was emitted by LS I +61°303, rather than by nearby sources or has a diffuse origin The weights are calculated using the Science Tool gtsrcprob, adopting the best spectral-spatial models obtained by the binned likelihood fits described in the previous section. Before calculating the power spectrum, we also applied to the light curve the exposure weighting described in Corbet et al. 2007. Fig. 4 shows the power spectra calculated in each of the time intervals. The vertical line marks the orbital period (as in Gregory 2002). The y-axis in the periodograms is given in average

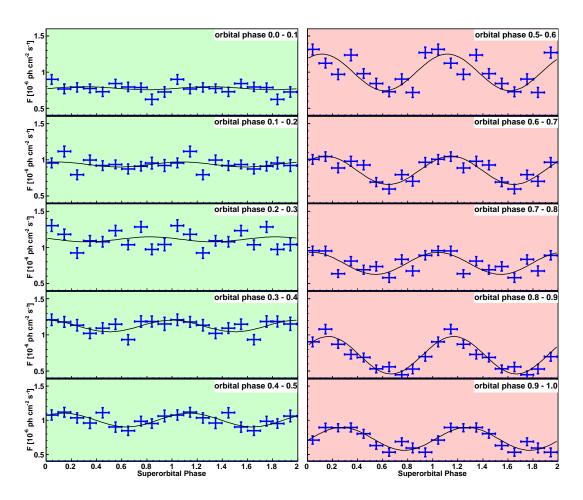


Fig. 3.— The evolution of the  $\gamma$ -ray flux (above 100 MeV) from LS I +61°303 at fixed orbital phases as a function of the superorbital phase. The data points are repeated over two superorbital periods for the sake of clarity. The left panels represent the region of the orbit near periastron (located at phase  $\sim 0.3$ , see Fig. 1) where the data are compatible with no superorbital variability beyond  $3\sigma$ .). The right panels, instead, are regions close to apastron. The black line in each of the panels is a sinusoidal function fit to the data points, with a fixed period of 1667 days.

power units, which converts the original spectrum in units of (ph cm<sup>-2</sup> s<sup>-1</sup>)<sup>2</sup> by normalizing it with the average of the power over all the frequencies < P >. In this way, the units are directly linked to the significance of the peak, which for a peak of power  $\bar{P}$  is computed as  $\operatorname{Prob}(P > \bar{P}) = \exp(-\bar{P}/<P)$  (Scargle 1982). These average power values are plotted in Fig. 2. A significant peak is detected at the orbital period, but not in all time intervals. Note that in some of the panels of Fig. 4 there appears to be a shift of the 26.5-day peak, even though it is within the fundamental frequency  $(1/T_{obs})$  of the orbital period. A claim that the period shift of these peaks is significant would then imply a severe oversampling of the Fourier resolution, which for the duration of this dataset is 3.84 days. The shifted peaks are not significant either in the single-trial (looking for an specific frequency) or in the all-trials probability analysis of these power spectra. Thus, we have now found that along the time covered by our observations, the power spectrum peak at the orbital period is significant only at superorbital phases  $\sim 0.5 - 1.0$ . At other superorbital phases, the peak is absent or has a significance less than  $3\sigma$ .

## 4. Discussion

Over the last two decades, systematic monitoring of many Be X-ray systems allowed the discovery of many cases of superorbital cycles (see, e.g., Alcock et al. 2001, Rajoelimanana et al. 2011). Thus, in order to connect the discovered  $\gamma$ -ray observational pattern to conditions that vary over the superorbit, a quasi-cyclical expansion and shrinking of the circumstellar disc of a Be star may offer an alternative (e.g., Negueruela et al. 2001). The sizes of the stellar discs of Be stars are hypothesized to correlate with the equivalent width (EW) of the H $\alpha$  emission line (e.g., Grundstrom et al. 2006). In the longest-running campaign observing LS I +61°303 the maximum of the H $\alpha$  EW has been found in a broad region around superorbital phase 0.2 (see Zamanov et al. 1999; Zamanov & Martí 2000 and references therein). Thus, the X-ray (Li et al. 2012) as well as the  $\gamma$ -ray emission are enhanced at superorbital phases where maximal values of the H $\alpha$  EW have been measured. Concurrently, the power spectrum peak at the orbital period is less significant. This suggests that the disc may play a role in modulating both the gamma and the X-ray signals.

From the results in Fig. 3, one may conclude that in the periastron region, when the emission from the system is subject to essentially no superorbital variability, the conditions for the generation of gamma rays in the GeV range must not significantly change. We can thus assume that the compact object could be inside or severely affected by the Be disc matter when it is closer to the companion star (i.e., at orbital phases 0.0 to 0.5), for all superorbital phases. If this is the case, even when the EW of the H $\alpha$  line (and thus the

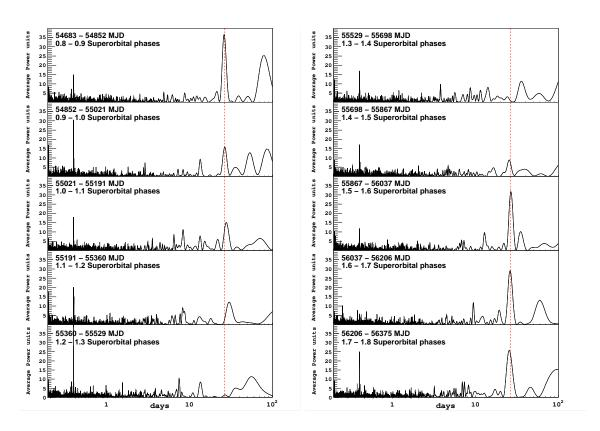


Fig. 4.— Periodogram of the  $\gamma$ -ray data for different time intervals. The dashed line marks the orbital period of LS I +61°303.

radius within which the disc influences) changes by a factor of a few along the superorbital period  $^3$ , this does not necessarily imply a significant change in the  $\gamma$ -ray modulation above the sensitivity of *Fermi*-LAT when the compact object is near periastron. However, in a two-component model typically assumed for Be stellar winds (an equatorial wind generating the disc, and a polar outflow) the conditions in the apastron region (e.g., the pressure exerted by the wind, or the mass gravitationally captured by the compact object) could change by more than 3 orders of magnitude if one or the other component dominates (see, e.g., Gregory & Neish 2002 and references therein). In such a case, it is reasonable to suppose that the GeV emission would be affected at an observable level.

We notice from Fig. 3 that between the orbital phase ranges 0.9–1.0 and 0.0–0.1 there is a significant change of the long-term behavior of the  $\gamma$ -ray emission. Closer to periastron the flux evolution flattens. We can then estimate the radius at which the matter in the disc of the Be star produces a stable influence with time by computing the system separation at orbital phase  $\sim 0.1$ . Using the ephemeris given by Aragona et al. (2009), we obtain a separation of  $\sim 9R_s$ , where  $R_s$  is the stellar radius of the Be star. On the other hand, from the fact that the maximal amplitude of the superorbital variability is before and after the apastron of the system, the system separation at orbital phases 0.7 and 0.9 ( $\sim 13R_s$ ) could also have a physical meaning. It is a qualitative upper limit to the influence of the matter in the equatorial outflow when maximally enhanced by the long-term change of the stellar mass-loss rate.

The ratio between what appears to be the maximal and the stable radii of influence of the disc matter is consistent with a possible increase of the EW of the H $\alpha$  line. Outer radii of discs in binaries are expected to be truncated by the gravitational influence of their compact companions; at the periastron distances in systems of high eccentricity, and by resonances between the orbital period and the disc gas rotational periods in the low-eccentricity systems (Okazaki et al. 2001). LS I +61°303 is a system between these two cases. The effects of the Be star's rotation, which have only recently started to be taken into account, may modify this conclusion, predicting disc sizes in excess of 10  $R_s$  (Lee 2013). Assuming the relation between disc size and the EW of the H $\alpha$  by (Grundstrom et al. 2006), and not taking into account rotation effects, typical values of the EW of LS I +61°303 would lead to an estimation of the disc radius of the order of the periastron distance (Grundstrom et al. 2007). Simulations indicate that tidal pulls at periastron can lead to the development of large spiral waves in

<sup>&</sup>lt;sup>3</sup>The mass-loss rate variations from the Be star in LS I +61°303 were estimated as the ratio between maximal and minimal values of its radio emission (a factor of  $\sim$ 5 was determined by (Gregory et al. 1989; Gregory & Neish 2002)) or its Hα measurements, which span factors of  $\sim$ 1.5 to 5 (Zamanov et al. 1999; Grundstrom et al. 2007; Zamanov et al. 2007; Mc Swain et al. 2010).

the disc that can extend far beyond the truncation radius and out to the vicinity of the companion (see e.g., Okazaki et al. 2001), promoting accretion (Grundstrom et al. 2007). The  $\gamma$ -ray data apparently provide a window to infer the extent of these waves.

Depending on the period and dipolar magnetic field, a highly-magnetized neutron star can transition between states along the orbital evolution of LS I +61°303, changing its behavior from propeller (near periastron) to ejector (near apastron) along each orbit (Zamanov et al. 2001; Torres et al. 2012; Papitto et al. 2012). These changes of state can be affected by the superorbital variability, since for a larger disc-influence radius, the system will remain in the same environment for a longer time (Papitto et al. 2012). The orbital variability is consequently reduced, leading to the disappearance of the orbital peak in the power spectrum (Torres et al. 2012). The data presented in this report will put the details of this model to the test while opening the  $\gamma$ -ray window for studying the discs of Be binaries.

The Fermi LAT Collaboration acknowledges support from a number of agencies and institutes for both development and the operation of the LAT as well as scientific data analysis. These include NASA and the U.S. Department of Energy (United States); CEA/Irfu and IN2P3/CNRS (France); ASI and INFN (Italy); MEXT, KEK, and JAXA (Japan); and the K. A. Wallenberg Foundation, the Swedish Research Council and the National Space Board (Sweden). Additional support from INAF in Italy and CNES in France for science analysis during the operations phase is also gratefully acknowledged. Additional support of this work comes from grants AYA2012-39303, SGR2009-811, and iLINK2011-0303. DFT was additionally supported by a Friedrich Wilhelm Bessel Award of the Alexander von Humboldt Foundation.

## REFERENCES

Abdo, A. A., Ackermann, M., Ajello, M., et al. 2009, ApJ 701, L123

Albert, J., Aliu, E., Anderhub, H., et al. 2006, Science 312, 1771

Albert, J., Aliu, E., Anderhub, H., et al. 2008, ApJ 684, 1351

Alcock, C., Allsman, R. A., Alves, D. R., et al. 2001, MNRAS 321, 678

Aragona, C., McSwain, M. V., Grundstrom, E. D., Marsh, A. N., Roettenbacher, R. M., Hessler, K. M., Boyajian, T. S., & Ray, P. S. 2009, ApJ 698, 514

Bosch-Ramon, V., & Khangulyan, D. 2009, Int. J. Mod. Phys. D 18, 347

Chernyakova, M., Neronov, A., Molkov, S., Malyshev, D., Lutovinov, A., Pooley, G. 2012, ApJ 747, L29

Corbet, R. H. D., Markwardt, C. B., & Tueller, J. 2007, ApJ 655, 458

Dubus, G. 2006, A&A 456, 801

Gregory, P. C. 2002, ApJ 575, 427 (2002).

Gregory, P. C., Xu, H.-J., Bachhouse, C. J., & Reid, A. 1989, ApJ 339, 1054

Gregory, P. C., & Neish, C. 2002, ApJ 580, 1133

Grundstrom, E. D., & Gies, D. R. 2006, ApJ 651, L53

Grundstrom, E. D., Caballero-Nieves, S. M., Gies, D. R., et al. 2007, ApJ 656, 437

Hadasch, D., Torres, D. F., Tanaka, T., et al. 2012, ApJ 749, 54

Lee, U. 2013, *PASJ* in press, arXiv:1304.6471

Li, J., Torres, D. F., Zhang, S., et al. 2012, ApJ 744, L13

Lomb, N. R. 1976, Ap&SS 39, 447

Maraschi, L., & Treves, A. 1981, MNRAS 194, 1P

McSwain, M. V., Grundstrom, E. D., Gies, D. R., & Ray, P. S. 2010, ApJ 724, 379

Mattox, J. R., et al. 1986, ApJ 461, 396

Negueruela, I. Okazaki, A. T., Fabregat, J., Coe, M. J., Munari, U., Tomov, T. 2001, A&A 369, 117

Nolan, P. L., et al. 2012, Astrophys. J. Suppl. 199, 31

Okazaki, A. T., & Negueruela, I. 2001, A&A 377, 161

Papitto A., Torres D. F., & Rea N. 2012, ApJ 756, 188

Rajoelimanana, A. F., Charles, P. A., & Udalski, A. 2011, MNRAS 413, 1600

Scargle, J. D. 1982, ApJ 263, 835

Torres, D. F., Zhang, S., Li, J., et al. 2010, ApJ 719, L104

Torres, D. F., Rea, N., Esposito, P., et al. 2012, ApJ 744, 106

- Zamanov, R. K., Martí, J., Paredes, J. M., et al. 1999, A&A 351, 543
- Zamanov, R. K., & Martí, J. M. 2000, A&A 358, 55
- Zamanov, R. K., Martí, J. M., & Marziani, P. 2001, The Second National Conf. Astrophysics of Compact Objects, p. 50, arXiv:astro-ph/0110114
- Zamanov, R. K., Stoyanov, K. A., & Tomov, N. A. 2007, Information Bulletin on Variable stars 5776
- Zhang, S., Torres, D. F., Li, J., et al. 2010, MNRAS 408, 642

This preprint was prepared with the AAS  $\mbox{\sc LAT}_{\mbox{\sc EX}}\mbox{\sc X}$  macros v5.2.

Table 1: Quality of the fitting results corresponding to Fig. 3 (top panel) and sinusoidal fitting parameters for the flux near apastron (bottom panel).

Orbital	$\chi^2$ , ndf	Constant Fit	$\chi^2$ , ndf	Sine Fit	Prob. improvement
Phase	(constant)	Probability	(sine)	Probability	by chance
0.0-0.1	10, 9	$3.2 \times 10^{-1}$	10, 7	$1.9 \times 10^{-1}$	1.0
0.1 – 0.2	13, 9	$1.8 \times 10^{-1}$	12, 7	$1.1\times10^{-1}$	1.0
0.2 – 0.3	27, 9	$1.4 \times 10^{-3}$	26, 7	$5.0 \times 10^{-4}$	0.7
0.3 – 0.4	13, 9	$1.6 \times 10^{-1}$	8, 7	$3.6 \times 10^{-1}$	$7.0 \times 10^{-2}$
0.4 – 0.5	15, 9	$9.9 \times 10^{-2}$	6, 7	$5.4 \times 10^{-1}$	$1.2 \times 10^{-2}$
0.5 – 0.6	84, 9	$2.8 \times 10^{-14}$	23, 7	$2.0 \times 10^{-3}$	$< 1.0 \times 10^{-7}$
0.6 – 0.7	50, 9	$8.1 \times 10^{-8}$	10, 7	$2.2\times10^{-1}$	$< 1.0 \times 10^{-7}$
0.7 – 0.8	41, 9	$6.1 \times 10^{-6}$	18, 7	$1.0 \times 10^{-2}$	$1.4 \times 10^{-5}$
0.8 – 0.9	100, 9	$2.4 \times 10^{-17}$	8, 7	$3.0 \times 10^{-1}$	$< 1.0 \times 10^{-7}$
0.9 - 1.0	50, 9	$9.1 \times 10^{-8}$	10, 7	$2.2\times10^{-1}$	$< 1.0 \times 10^{-7}$
Orbital	$F_0$	A	φ		
Phase	$[10^{-6} \text{ ph cm}^{-2} \text{ s}^{-1}]$	$[10^{-6} \text{ ph cm}^{-2} \text{ s}^{-1}]$	,		
0.5-0.6	$1.00\pm0.03$	$0.25 \pm 0.03$	$0.87 \pm 0.03$		
0.6 – 0.7	$0.85 {\pm} 0.02$	$0.20 \pm 0.03$	$0.90 \pm 0.02$		
0.7 – 0.8	$0.78 \pm 0.02$	$0.15 \pm 0.03$	$0.79 \pm 0.03$		
0.8 – 0.9	$0.72 \pm 0.03$	$0.26 \pm 0.03$	$0.92 \pm 0.03$		
0.9–1.0	$0.73 \pm 0.02$	$0.17 \pm 0.03$	$0.02 {\pm} 0.04$		